Applied Catalysis A: General 470 (2014) 420–426

Contents lists available at ScienceDirect

Applied Catalysis A: General

journal homepage: www.elsevier.com/locate/apcata

High catalytic performance of surfactant-directed nanocrystalline zeolites for liquid-phase Friedel–Crafts alkylation of benzene due to external surfaces

Jeong-Chul Kim [a,b], Kanghee Cho [b], Ryong Ryoo [b,c,*]

[a] Graduate School of Nanoscience and Technology, KAIST, Daejeon 305-701, Republic of Korea
[b] Center for Nanomaterials and Chemical Reactions, Institute for Basic Science (IBS), Daejeon 305-701, Republic of Korea
[c] Department of Chemistry, KAIST, Daejeon 305-701, Republic of Korea

ARTICLE INFO

Article history:
Received 27 September 2013
Received in revised form 8 November 2013
Accepted 13 November 2013
Available online 22 November 2013

Keywords:
Nanomorphic zeolite
Mesoporous zeolite
Zeolite external acidity
Friedel–Crafts alkylation
Catalytic lifetime

ABSTRACT

Beta zeolite is known as an efficient catalyst for Friedel–Crafts alkylation. In liquid phase reactions, however, beta zeolite catalyst is often deactivated rapidly. We discovered that the maximum possible catalytic turnovers in benzene alkylation with benzyl alcohol could be increased by six times by using a beta zeolite with a nanosponge-like morphology, in comparison to bulk beta zeolites. The nanomorphic zeolite was obtained using a hydrothermal synthesis method which uses multiammonium surfactants as a meso–micro hierarchical structure-directing agent. The origins of the high catalytic performance were investigated by measuring the catalytic conversions after selectively poisoning acid sites located on external surfaces and in internal micropores selectively. The result indicated that the high catalytic performance was due to the alkylation reactions occurring on external surfaces. External active sites were able to perform the catalytic function even after active sites inside the zeolite micropores were deactivated. Similar results were obtained with other nanomorphic zeolites such as MFI nanosheets, MTW nanosponge and MRE nanosponge.

1. Introduction

Friedel–Crafts (FC) alkylation is one of the most important chemical processes to produce value-added aromatic compounds through the formation of new C–C bonds between aromatic molecules and alkylating agents such as olefins, alkyl halides and alcohols [1–3]. Many FC alkylated aromatic products are used as key intermediates for the production of petrochemicals, cosmetics, dyes and pharmaceuticals [2–5]. FC alkylation can be catalyzed by both Lewis and Brönsted acids. The catalysts can be used as homogeneously dissolved components in reaction media (i.e., homogeneous catalysts), or as solid acids (heterogeneous catalysts) [1–3,6–9]. Among the heterogeneous FC alkylation catalysts, zeolites are widely used in industrial processes, due to many advantages such as strong acidity, shape selectivity, high stability and easy regenerability [10].

In petrochemical processes, FC alkylation for easily volatile products such as cumene synthesis and toluene alkylation are operated in gas phase, continuous plug-flow mode using beta zeolite catalyst [11–15]. The advantage of this mode is high producibility and long catalytic lifetime. However, for low volatile organic products, FC alkylation is difficult to operate in gas phase. Instead, the alkylation can be operated in liquid phase using a batch reactor [16,17]. In many previous works on liquid phase FC alkylation, the conversion of reactants was often reported to reach almost 100% using beta zeolite as a catalyst [18]. The benzylation of benzene with benzyl alcohol is a typical example. This reaction is often reported to go to almost 100% conversion with zeolites or mesoporous aluminosilicate catalysts [19–24]. If a limited amount of catalyst is used, however, high conversion is difficult to achieve in liquid phase. The conversion does not increase beyond a certain value even if a very long reaction time is given. To show this, we measured the conversion of benzyl alcohol (limiting agent) with various amounts of reactants per catalyst using a conventional aluminosilicates beta zeolite. The result indicated that the maximum possible benzyl alcohol conversion (%) decreased against the reactant-to-Al ratio. We then converted the maximum conversion to the number of benzyl alcohol molecules per Al atom contained in the zeolite, and plotted the conversion per Al (CPA) as a function of the reactant amount. This plot showed that the CPA stopped increasing after reaching a maximum value about 40. That is, the zeolite catalyst was completely deactivated after CPA reaching 40.

* Corresponding author. Tel.: +82 42 350 2830; fax: +82 42 350 8130.
E-mail address: rryoo@kaist.ac.kr (R. Ryoo).

0926-860X/$ – see front matter © 2013 Published by Elsevier B.V.
http://dx.doi.org/10.1016/j.apcata.2013.11.019

The purpose of the present work was to investigate why the liquid-phase FC alkylation zeolite catalyst was so rapidly deactivated, and therefore, to seek a solution to the deactivation problem. We approached the problem, focusing particularly on the effect of zeolite particle size. We noted that zeolites for catalytic applications are normally composed of crystallites on a micrometer scale (~1 μm). Despite so small particle sizes, even such micro-crystallites are still much larger than the diameter of the internal micropores (<1 nm) that constitute the crystal structure. Such zeolites are called bulk zeolites, and their external crystal surface area is very small as compared to internal surfaces corresponding to a large number of micropores. When a bulk beta zeolite is used as a catalyst, the benzyl alcohol–benzene reaction can occur mostly inside the micropores. Reactions on the external surfaces can be disregarded, due to the relatively small surface area. The phenomenon is similar in various reactions where bulk zeolites are used as catalysts [25,26]. On the other hand, in nanomorphic zeolites (i.e., zeolites with nanoscale morphologies), the catalytic function of the external surfaces can be quite significant, as recently reported by Kim et al. [27]. Kim et al. synthesized MTW, MRE and beta zeolites with nanosponge-like morphologies via a recently-developed synthesis route which used multiammonium surfactants as meso–micro dual structure-directing agents (SDAs). These nanomorphic zeolites exhibited superior catalytic performance to their bulk counterparts in a gas-phase cumene synthesis study. It was particularly notable that the nanomorphic zeolites maintained high catalytic activities for a long time, whereas bulk zeolites lost activity almost completely. Kim et al. were able to separate the catalytic deactivation curve into two exponential functions. Based on this analysis, they attributed the high catalytic performance of the nanomorphic zeolites to benzene alkylation reactions occurring mainly at catalytic sites that were located at external surfaces. If this was correct, the catalytic reactions in these zeolites should have occurred dominantly at the external active sites rather than the internal acid sites. In addition, the external active sites exhibited much longer catalytic lifetimes than the internal sites. Nevertheless, such effects of external acid sites to the catalytic performances were not yet generally confirmed in other zeolite catalysis, particularly in liquid-phase FC alkylation.

For the purposes of the present research, four structure types of zeolite (i.e., beta, MTW, MRE, and MFI) with nanosponge morphologies were synthesized via the multi-ammonium surfactant route [27,28]. These nanomorphic zeolites were characterized in terms of their catalytic conversion rates and the maximum possible conversions in liquid-phase FC alkylation of benzene with benzyl alcohol. Efforts were made to quantify the catalytic conversions taking place on the external surfaces in comparison to reactions occurring inside micropores, using a nanomorphic beta zeolite sample. One strategy to this end was to treat the zeolite sample with triphenylphosphine before benzylation reaction measurement. Triphenylphosphine was a strong base molecule so that it could poison acid sites in a zeolite by strong chemisorption. The poisoning was limited to the external surfaces as the molecule was too large to enter a micropore aperture in a beta zeolite. Another strategy was to expose the zeolite sample to a high-temperature gas flow containing benzene and *i*-propene, prior to benzylation. This treatment could deactivate the internal catalytic sites more rapidly than the external sites due to the preferential deposition of coke in micropores [29,30]. We analyzed the result of the catalytic reaction measurements after such selective deactivation treatments. This investigation indicated that the cause for the rapid catalytic deactivation of bulk beta zeolites in liquid-phase FC alkylations was due to internal pore blockage by the bulky side products. Compared to the internal sites, the external sites were very slowly deactivated. Thus, zeolite synthesis in nanomorphic form turned out as an effective means of achieving high catalytic turnovers in the liquid-phase benzylation reaction.

2. Experimental

2.1. Material preparation

Nanomorphic zeolite samples were synthesized with multi-ammonium surfactant SDAs as described elsewhere [27,28]. Beta, MTW and MRE zeolites were synthesized using the same SDA, $[C_{22}H_{45}–N^+(CH_3)_2–C_6H_{12}–N^+(CH_3)_2–CH_2–(C_6H_4)–CH_2–N^+(CH_3)_2–C_6H_{12}–N^+(CH_3)_2–CH_2–(C_6H_4)–CH_2–N^+(CH_3)_2–C_6H_{12}–N^+(CH_3)_2–C_{22}H_{45}](Br^-)_2(Cl^-)_4$. Tetraethylorthosilicate (TEOS, 95%, Junsei) was used as the silica source for the nanomorphic zeolite samples. Sodium aluminate (53 wt%, Sigma-Aldrich) was the alumina source. The details of the synthesis conditions were differently optimized for each zeolite structure. The optimized synthesis conditions are the same as described by Kim et al. [27]. For MFI zeolite, the SDA was $[C_{16}H_{33}–N^+(CH_3)_2–C_6H_{12}–N^+(CH_3)_2–C_6H_{13}(Br^-)_2]$. Sodium silicate solution (Si/Na = 1.75, 15 wt% SiO_2) was used as a silica source for the MFI zeolite. Sodium aluminate (53wt%, Sigma-Aldrich) was used as an alumina source. The synthesis conditions were the same as those reported by Kim et al. [28]. These nanomorphic zeolite samples are denoted as nanozeolites. Their corresponding bulk samples were also synthesized following the procedures [28,31–33]. An Al-MCM-41 sample was prepared via the postsynthetic incorporation of Al, following a procedure reported in the literature [23]. All zeolite and Al-MCM-41 samples were calcined in air at 853 K after hydrothermal synthesis.

2.2. Characterization

Powder X-ray diffraction (XRD) patterns were measured with a Rigaku Multiflex diffractometer equipped with Cu *K*α radiation (30 kV, 40 mA). The Ar adsorption isotherms were measured at the liquid argon temperature with an ASAP 2020 volumetric adsorption analyzer [34]. Si/Al ratios were determined by inductively coupled plasma-atomic emission spectroscopy (ICP-AES) using an OPTIMA 4300 DV instrument (Perkin Elmer). Scanning electron micrographs (SEM) images were taken with a Hitachi S-4800 microscope operating at 2 kV without a metal coating. Transmission electron micrographs (TEM) images were obtained using a TecnaiG2 F30 at an operating voltage of 300 kV. ^{31}P NMR spectra were acquired in a solid state with magic angle spinning (MAS) using a Bruker AVANCE400WB spectrometer at room temperature, following the method reported in the literature [35].

2.3. Catalytic measurements

Calcined zeolites in powder form were slurried in a 1-M NH_4NO_3 solution three times in total for the ion exchange into NH_4^+. The zeolites were calcined again in air at 823 K to convert to a H^+-ion-exchanged form. The liquid-phase FC alkylation reaction was performed using a Pyrex batch reactor. Typically, 50 mg of H^+-form zeolite was degassed at 573 K. This sample was added to a Pyrex glass reactor that contained 190 mmol of benzene and (7.2, 14.4, or 28.8) mmol of benzyl alcohol. The mixing was carried out in a glove box to prevent moisture contamination. The reactor temperature was quickly (<3 min) increased to 353 K under magnetic stirring. Small aliquots (0.1 ml) of samples were taken at various times afterward. At each sampling, the solid catalysts were filtered out after immediate cooling to room temperature. The liquid phase was analyzed on a gas chromatograph equipped with a flame

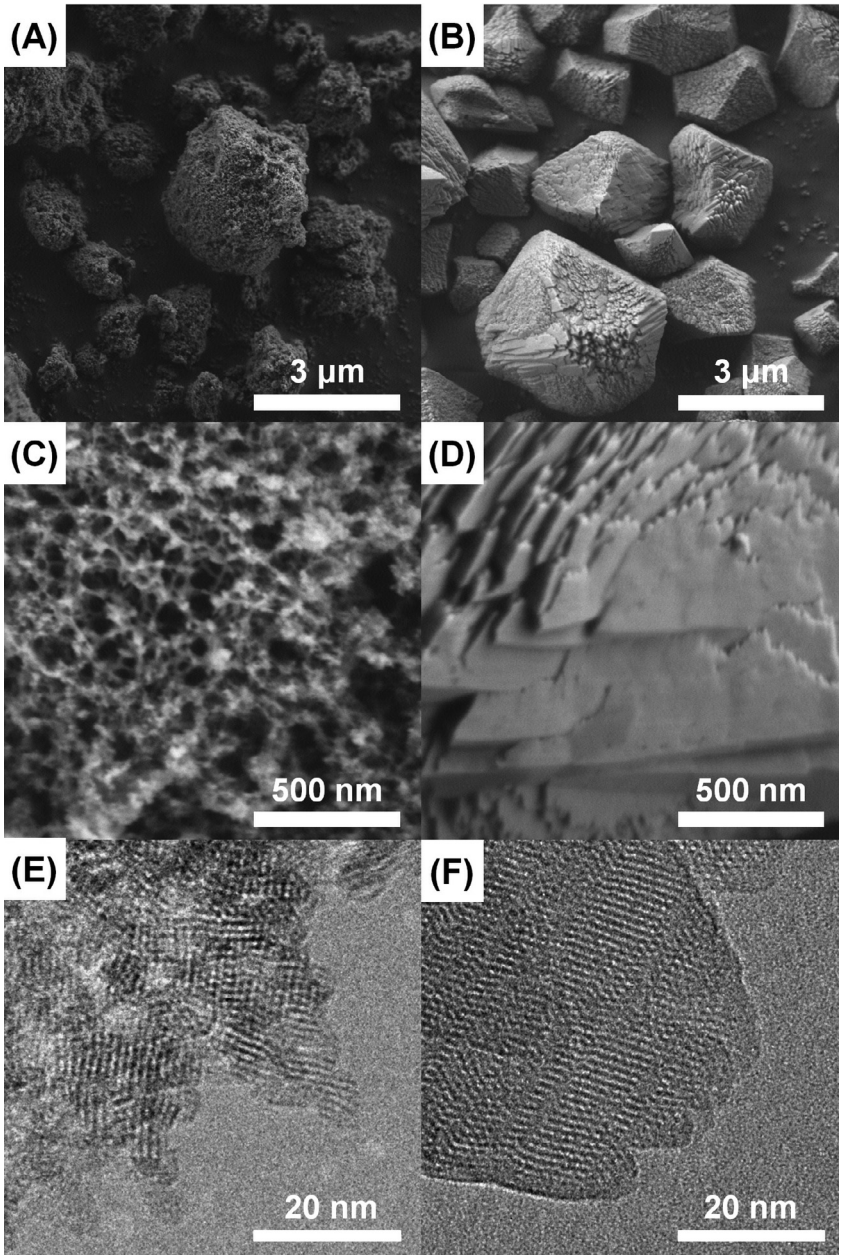

Fig. 1. EM micrographs of nano beta (left column) and bulk beta (right column): SEM images with low-magnification (a and b) or high-magnification (c and d), and high-magnification TEM images (e and f).

ionization detector and a HP–1 column (Agilent, 30 m long, 0.32 mm i.d., and 1 μm thick coating).

3. Results and discussion

3.1. Large external surface area of beta zeolite nanosponge

Fig. 1 shows representative SEM and TEM images taken from beta zeolite samples. The EM images of the nano zeolite indicate that the sample was composed of very thin (approximately 20 nm) beta zeolite crystals. The nanocrystals were randomly and loosely interconnected to form a nanosponge-like mesoporous assembly. On the other hand, the SEM images of the bulk zeolite indicate that the zeolite was composed of particles of approximately 2 μm in diameter. The external surface of the particles showed many crystal steps and terraces, but overall, the surfaces did not indicate the presence of mesopores. Fig. 2 shows the XRD patterns and argon adsorption isotherms measured at the liquid argon temperature (87 K). The XRD pattern of the bulk beta zeolite exhibited several representative Bragg reflections corresponding to the typical beta zeolite structure with polymorphs. The XRD peaks appearing around $2\theta = 7.5^\circ$ were somewhat broad, which was due to the presence of more than two polymorphs. Except this peak, the XRD pattern of the bulk zeolite exhibited quite sharp peaks. Furthermore, there was no detectable background increase in the 2θ region between 15° and 25° that could indicate presence of any amorphous phases. Compared to the bulk zeolite, the nano beta sample showed only two detectable peaks ($2\theta = 7.5^\circ$ and 22°). These peaks were very broad, but nevertheless, they were consistent with (1 0 1) and (3 0 2) reflections of a beta zeolite. The broad peak widths should be attributed to the small crystal domains in the nanocrystalline morphologies. Other reflections were difficult to identify due to their low intensities in addition to the peak broadening [37].

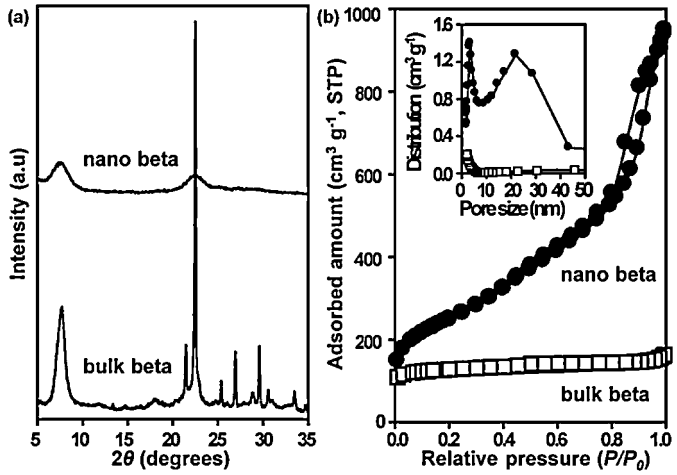

Fig. 2. Powder XRD patterns (a) and argon adsorption isotherms (b) of bulk and nano beta zeolites. Inset of (b) is pore size distributions corresponding to the adsorption branch of nano beta and bulk beta.

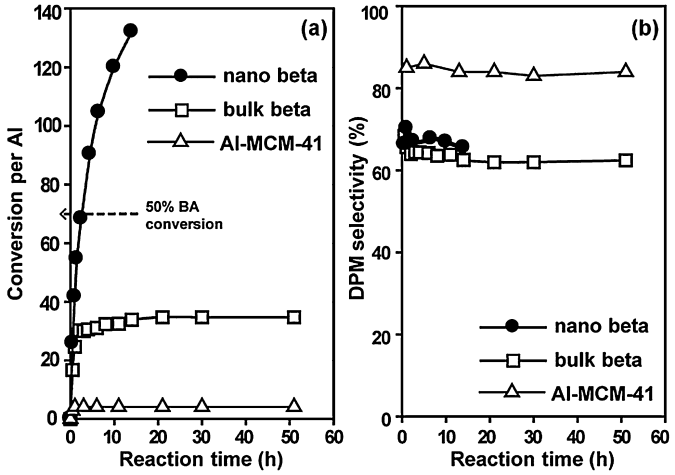

Fig. 3. Conversion per Al (a) and Diphenylmethane (desired product, in short, 'DPM') selectivity (b) plotted as a function of reaction time: nano beta (●), bulk beta (□) and Al-MCM-41 (△). Reaction condition: 7.2 mmol of benzyl alcohol, 190 mmol of benzene, 50 mg of catalyst, 353 K.

Argon adsorption isotherm of bulk zeolite exhibited a very sharp increase in the low-pressure region of $P/P_0 < 0.1$, which is interpreted as due to the argon filling in the micropores. Such an isotherm shape is a typical feature of microporous material. The micropore diameters were determined from the isotherm in the region of $P/P_0 < 0.1$ using nonlocal density functional theory. A very sharp distribution peak appeared at 0.70 nm. On the other hand, the isotherm of nano zeolite showed another jump in the medium-pressure region of $0.4 < P/P_0 < 0.5$, as well as a sharp increase in the low-pressure region. The former is due to capillary condensation in the mesopores. The latter is due to argon filling in quite uniform micropore with an average diameter of 0.70 nm as in bulk beta zeolite. The Barrett–Joyner–Halenda algorithm was used to determine the size of the mesopores. The mesopore-size distribution obtained in this manner showed a narrow peak center at 4.5 nm. The specific surface area of the two zeolite samples was determined by the Brunauer–Emmett–Teller (BET) method (see Table 1). BET-specific areas of bulk and nano beta showed a significant difference: 460 $m^2\ g^{-1}$ for bulk and 930 $m^2\ g^{-1}$ for nano zeolites. Such a difference is due to a significant increase of the external surface area that was exposed to mesopores in the nano beta zeolite. The following external surface areas were determined according to the *t*-plot method: 50 $m^2\ g^{-1}$ for bulk and 700 $m^2\ g^{-1}$ for nano beta.

The Si/Al ratios of nano and bulk beta zeolites were 16 and 15, respectively, according to elemental analysis using inductively-coupled plasma atomic emission spectroscopy (Table 1). Solid Al NMR measurement was performed for zeolite beta samples, showing that almost all aluminum atoms in two zeolites were incorporated in tetrahedral sites of two zeolites. The elemental analysis and Al NMR investigation indicated that two zeolites contained a similar number of Brönsted acid sites in a unit weight. The strength and distribution of the Brönsted acid in two zeolites were analyzed by solid-state ^{31}P NMR spectroscopy using phosphine oxides as a probe molecule, following previous works [38,39]. This technique was known as an effective method to quantify the concentration of the acid sites at different locations (e.g., at internal micropores or external surfaces) and to classify the acid groups according to their strengths [27,35]. Trimethylphosphineoxide, which is much smaller than the micropore size of zeolite beta, was used as probe molecule to evaluate the total amount of Brönsted acid over the entire region of the zeolite. Table 1 includes the results of ^{31}P NMR measurement, showing that that bulk and nano beta had a similar amount of Brönsted acid, which is in good agreement with elemental analysis and Al NMR measurement. On the other hand, the number of external acid sites was evaluated by ^{31}P NMR spectroscopy, adsorbing tributylphosphine oxide into the zeolites. Table 1 shows that nano beta contained 34% of the total Brönsted acids at the external surface, whereas only 5% of the total Brönsted acids were located at the external surfaces of bulk beta. This result shows similar results with those of MFI zeolite nanosheets synthesized via the same synthesis approach, as shown in a previous report [35].

3.2. High catalytic turnover of zeolite beta nanosponge

The catalytic properties of bulk and nano beta zeolites were investigated in the liquid-phase benzylation of benzene with benzyl alcohol (BA) where Brönsted acid sites are used as active sites. Al-MCM-41 with a Si/Al ratio of 15 was also tested in the benzylation as a catalyst containing very weak Brönsted acidity for comparison with the zeolite catalysts. Fig. 3a shows the catalytic results of two zeolite catalysts and Al-MCM-41 by the means of CPA plotted as a function of reaction time. Nano and bulk beta showed

Table 1
Physicochemical properties of the nano and bulk beta catalysts.

Catalysts	Si/Al[a]	S_{BET}[b] ($m^2\ g^{-1}$)	S_{ext}[c] ($m^2\ g^{-1}$)	V_{tot}[d] ($cm^3\ g^{-1}$)	BA_{ini}[e] ($\mu mol\ g^{-1}$)	BA_{ext}[f] ($\mu mol\ g^{-1}$)	BA_{ex}/BA_{tot}[g] (%)
Nano beta	16	930	700	1.40	644	326	34
Bulk beta	15	460	50	0.24	1090	55	4.8

[a] Si/Al mole ratio obtained from ICP/AES analysis.
[b] S_{BET} is the BET surface area obtained from Ar adsorption in relative pressure range (P/P_0) of 0.05–0.20.
[c] S_{ext} is the external surface area determined according to the *t*-plot method.
[d] V_{tot} is the total pore volume obtained at $P/P_0 = 0.95$.
[e] BA_{int} is the concentration of internal Brönsted acid sites, which was calculated by subtracting the concentration of external acid sites from that of total acid sites.
[f] BA_{ext} is the concentration of external Brönsted acid sites.
[g] BA_{ex}/BA_{tot} is the molar ratio of the external acids to total acids.

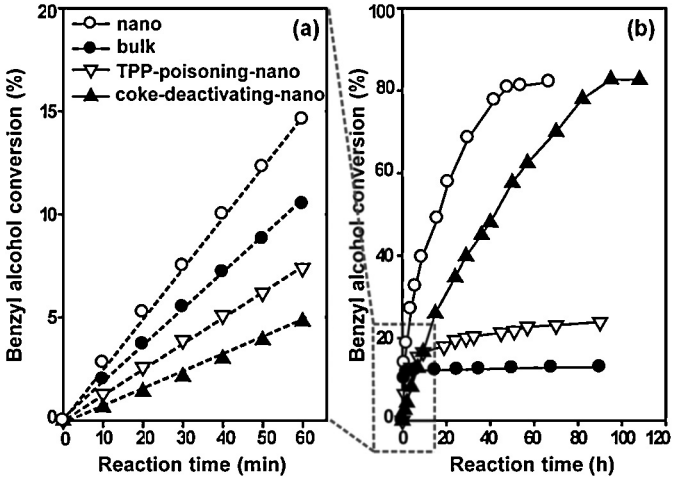

Fig. 4. Conversion of benzyl alcohol over bulk beta (●), nano beta (○), nano beta with external-acid poisoning by TPP (▽) and nano beta with micropore-blocking by coke (▲), plotted as a function of reaction times: 0–1 h (a) and 0–120 h (b). Reaction condition: 14.4 mmol of benzyl alcohol, 190 mmol of benzene, 10 mg of triphenylphosphine, 50 mg of fresh and coked catalyst, 353 K.

significant CPA with similar product selectivity (approximately 70% of the product mixture was diphenylmethane and the others were mostly dibenzyl ether, which was generated by self-condensation of BAs). In contrast to the zeolite catalysts, Al-MCM-41 exhibited insignificant value of CPA, and the value did not increase for long time of reaction. This result indicates that the liquid-phase benzylation reaction requires strong Brönsted acid sites of the crystalline zeolite framework, which is stronger than the acid sites in an amorphous framework [27,37].

As mentioned above, both zeolite betas are quite active catalysts in the liquid-phase benzylation reaction, but they showed significant difference in the maximum value of CPA (Fig. 3a). In the case of bulk beta, CPA increased gradually with the reaction time and converged to a maximum value of 35 (conversion of BA: 25%) in 2 h. This value did not further increase, although the reaction was continued for long time. On the other hand, the CPA of nano beta gradually increased up to 135. Considering the reaction condition, this value of CPA corresponds to almost 100% BA conversion. 100% conversion means that nano zeolite could be still active after converting all BA molecules. If more reactant was added, nano beta might exhibit much higher CPA value.

The catalytic investigation for the zeolite beta catalysts was also carried out with an increase in the amount of the reactant. Fig. 4 shows the catalytic result of the catalytic test with high dosing of the reactant (14.4 mmol). Fig. 4a shows plots of BA conversion early in the reaction time, and Fig. 4b shows conversion plots of the overall range of reaction time. Until 1 h of the benzylation reaction, the conversion rate of BA using nano and bulk beta increased linearly. At 1 h of the reaction, the two zeolites exhibited less than 15% conversion. In this situation, the catalytic activities of the catalysts could be directly compared by the conversion rates. The result indicates that nano beta shows 1.3 times the activity of bulk beta in the benzylation reaction. In the long period until 100 h (see Fig. 4b), the BA conversion rate of nano beta increased gradually for a long time (~50 h) and converged to 80%. On the other hand, bulk beta became deactivated rapidly to exhibit a maximum BA conversion of approximately 13%. Considering the initial amount of BA and the number of acid sites in the zeolites, the maximum CPAs of nano and bulk beta could be evaluated to 230 and 35, respectively. That is, CPA for nano beta was almost six times as much as CPA for bulk beta.

The difference in CPA of the two zeolites could be attributed to the different crystal size and, accordingly, the concentration of the Brönsted acid sites at the external surface of the zeolite. The bulk beta contains a negligible amount of the external acid sites so that the catalytic performance of the bulk zeolite could be explained by only the behavior of the internal acid site. In nano zeolite, however, a portion of external acid sites is not negligible, so the catalytic reaction occurring at the external surface should be significantly concerned in the catalytic performance (catalytic activity and lifetime) of the zeolite catalyst. The catalytic performance of the external surfaces might be different from that of the internal micropores. To understand the effect and contribution of each internal or external active site in affecting the catalytic results, the catalytic tests were performed under same conditions after selectively deactivating one of two different active sites in the nano beta [27,36]. The external acid sites of nano beta could be selectively deactivated by the chemisorption of triphenylphosphine (TPP) following a procedure reported in the literature [36]. ^{31}P NMR investigation was performed to count the number of TPP at the external acid sites of the treated sample, confirming that almost all external acid sites adsorbed strongly the TPP molecule (i.e., poisoning). However, the internal sites remained strongly acidic. After the TPP poisoning treatment, the nano zeolite was immediately tested in the liquid-phase benzylation reaction. During the reaction, the TPP adsorbed at the external surface was not dissolved into the reaction solution so that the external acid sites remained deactivated. Fig. 4a shows that the treated nano beta exhibited significant but somewhat smaller catalytic conversion than pristine nano beta, early in the reaction time (<1 h). The slight decrease of the catalytic activity is attributed to the deactivation of external acid sites that can act as catalytic sites in this reaction. However, the treated nano beta was very rapidly deactivated in comparison with pristine nano beta. The treated nano beta was deactivated as fast as bulk beta zeolite was, meaning that the internal acid sites of the nano beta exhibited very short catalytic lifetime like that of the bulk beta.

The internal acid sites of nano beta could be preferably deactivated through micropore-blocking by coke which was generated during benzene isopropylation reaction [27]. Benzene isopropylation was carried out in a fixed bed Pyrex reactor (10 mm inside diameter) with gas-phase continuous plug-flow mode ($WHSV_{benzene}$ = 8.8 $g_{benzene}$ $g_{catalyst}^{-1}$ h^{-1}). The reaction was continued until the micropores were completely filled with carbon species, which was confirmed by argon sorption analysis. ^{31}P NMR measurements were performed after adsorbing phosphonium probe molecules such as trimethylphosphine and tributylphosphine, which confirmed that treated nano beta lost almost all internal acid sites. The treated sample was also tested in the liquid-phase benzylation reaction without further treatment, and the catalytic conversion was plotted as a function of reaction time in Fig. 4. Fig. 4a shows that the treated nano beta exhibited somewhat less catalytic activity than pristine nano beta, early in the reaction time (<1 h). However, the catalytic conversion of treated nano beta increased gradually for a long time (80 h) and achieved as high of a maximum conversion as that of pristine nano beta. This result indicated that the external acids can act as active sites in liquid-phase catalytic benzylation and exhibit significantly long catalytic lifetime. This aspect of external acid sites resembles the previous results in a gas-phase cumene reaction [27]. The longer catalytic lifetime of nano beta than bulk beta in a liquid-phase benzylation reaction, as well as gas-phase cumene synthesis [27], could be attributed to the nano beta possessing a significant amount of such an external acid sites which exhibit long catalytic lifetime.

3.3. Catalytic deactivation by organic deposition

The conventional zeolite catalysts were known to deactivate rapidly in the liquid-phase FC alkylation reactions due to the deposition of organic species inside the micropores or at the external surfaces [26,40]. The organic species thereby block the access of

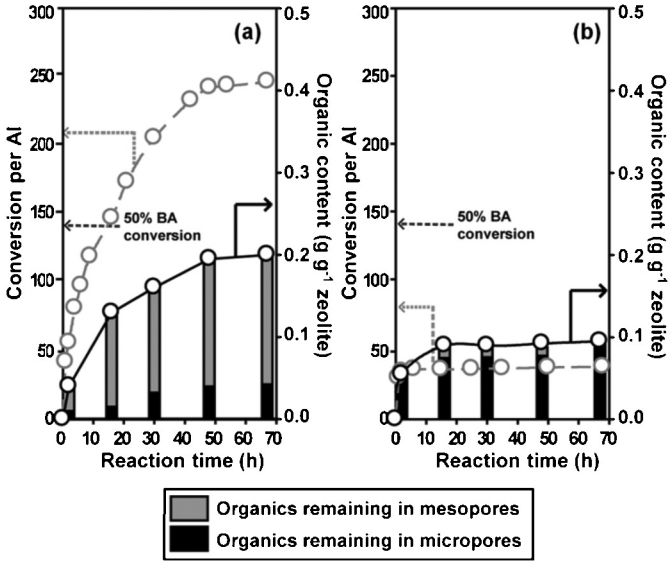

Fig. 5. Content and location of organic deposits on nano beta (a) and bulk beta (b) samples which were collected at various times of FC benzylation of benzene with benzyl alcohol. Gray line with hollow circle is conversion per Al over two zeolite beta catalysts plotted as a function of reaction time. Reaction condition: 14.4 mmol of benzyl alcohol, 190 mmol of benzene, 50 mg of catalyst, 353 K.

reactants into the active sites. Water, which was generated from the benzyl alcohol during the reaction, can also fill micropores quickly to hinder the access of reactants to active sites inside micropores [24,41,42]. In contrast to the carbon deposits, the water molecules can be reversibly removed from the active sites. The deactivation of nano zeolite might also be due to the covering the active sites by carbon residue and/or water. Nevertheless, as shown above, the nano zeolite exhibited much lower deactivation rate than the bulk zeolite in liquid-phase FC benzylation reaction. The difference might be due to different rate and location (e.g., in micropores or at the external surfaces) of the carbon species generated during the reaction. The generation of the organic residue in bulk and nano zeolites was observed in detail using argon sorption analysis, thermogravimetric analysis and elemental analysis. Experimental details of the coke analysis was described in Appendix A. The bulk and nano beta zeolites were sampled at various times of the benzylation reaction, and the nature and amounts of the organic residues generated in micropores and external surfaces were analyzed. As shown in Fig. 5, bulk beta generated the organic species almost in its micropores during the reaction. The organic species generated at the external surfaces was almost negligible. The content of the carbon deposit increased with the reaction time to achieve the maximum content of 0.1 g g^{-1} of the bulk beta. At this time, the catalyst was completely deactivated. This amount of the organic species could fill or completely block all of the whole micropores, which was confirmed by argon sorption analysis (see Fig. 5). In the case of nano beta, the amount of organic deposit also increased according to the reaction time, while the zeolite became increasingly deactivated. The differing features from bulk beta are that the organic component was more preferentially deposited in the mesopores (i.e., at the external surfaces) than inside the micropores. The amount of carbon deposits in the micropores of nano beta was smaller than that of bulk beta. After 20 h of the benzylation reaction, the total carbon contents and even the amount of only the external carbon species in the nano beta sample is larger than the maximum contents in total carbon deposits in bulk beta. Nevertheless, the nano beta catalyst was still active in the reaction. Since the mesopore size and volume is much larger than the micropores

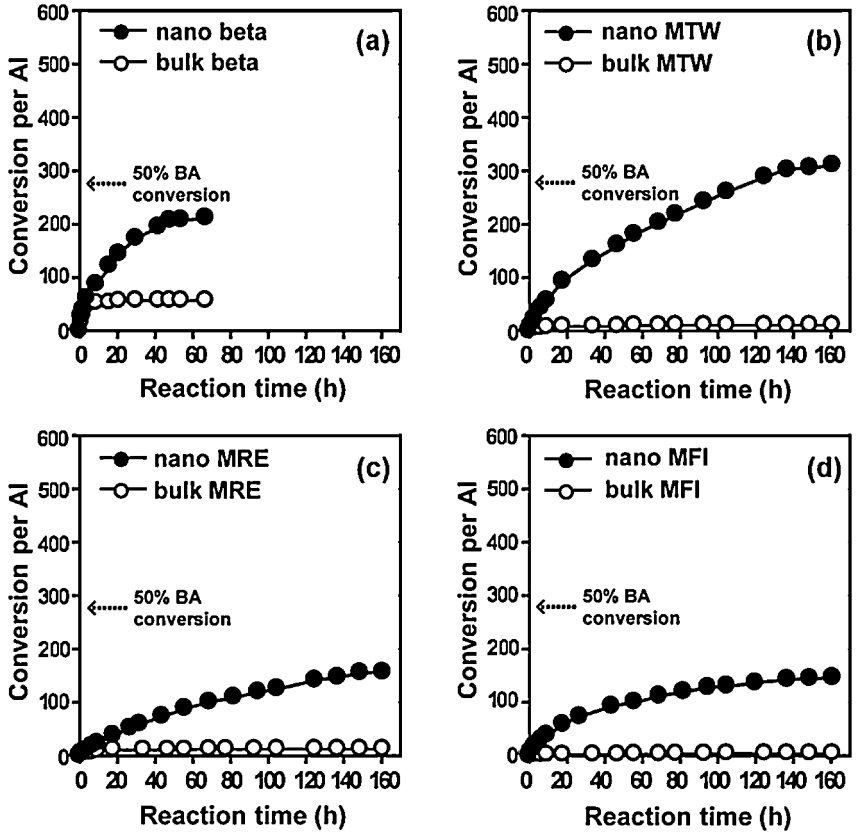

Fig. 6. Conversion per Al over beta (a), MTW (b), MRE (c), and MFI (d) zeolites plotted as a function of reaction time. Reaction condition: 28.8 mmol of benzyl alcohol, 190 mmol of benzene, 50 mg of catalyst, 353 K.

in the beta zeolite, the mesopore retained enough volume of empty space to make the reactants approach the active sites even after significant formation of carbon species. Argon sorption analysis confirmed that mesopore size and volume somewhat decreased but were still measurable after 20 h of the benzylation reaction.

The organic deposit in both nano beta and bulk beta was confirmed as various poly-alkylated aromatic compounds by LC–MS analysis. The poly-alkylated aromatics are likely to be generated via side reaction routes, such as the self-condensation of benzyl alcohol or the benzylation of benzene, and their repetition. Bulk beta contained relatively small-sized organic species consisting of two or three aromatic groups, whereas nano beta contained larger-sized organic species consisting of more than four aromatic groups, as well as the smaller poly-aromatic components. The large-sized organic molecules are somewhat larger than the micropore size. These species are probably located in the mesopores of nano beta. As compared to the small nanometer size of the mesopore, such a bulky molecule remains quite small in order to provide sufficient space for access of the reactant molecules.

3.4. High catalytic turnover of other types of nanomorphic zeolites

Liquid-phase benzylation reaction was also performed using other types of nano zeolites such as MTW-, MFI-, and MRE-types as catalysts. ^{31}P NMR investigation was performed for these nano zeolites, as done for zeolite beta samples. ^{31}P NMR result showed that these nano zeolites contained a significant number of strong Brönsted acid sites at the external surfaces than did their conventional bulk counterparts, as well as nano beta (Table S1). As well as the result of ^{31}P NMR investigation, other characterization results (XRD patterns, nitrogen sorption isotherm and EM micrographs) of all the zeolites were also shown in Appendix A. The reaction conditions were the same as those of the reaction using beta zeolite catalysts, except for the amount of BA (28.8 mmol). Fig. 6 summarizes the results of the catalytic investigation, showing a similar tendency with the beta zeolite system. All three nano zeolites (MTW, MFI, and MRE) exhibited much higher CPA than their bulk counterparts. It is noteworthy that bulk MTW, MFI, and MRE zeolites exhibited almost zero catalytic activities. In particular, the nano MTW zeolite exhibited somewhat higher catalytic activity, as nano beta was used as a catalyst under same catalytic conditions. From this catalytic investigation, we confirmed that the high content of external acid sites in nanomorphic zeolites, regardless of framework types, enables high catalytic performance in liquid-phase FC benzylation reaction for quite a long time. Also, it can be expected that all types of nanomorphic zeolites, especially nanomorphic MTW zeolite, will be highly applicable as high performance catalysts in the liquid FC benzylation reaction.

4. Conclusions

In this research, we discovered that the nanomorphic zeolites show higher catalytic activity for much longer times in liquid-phase FC benzylation than conventional bulk zeolites. Consequently, the nanomorphic zeolites exhibited at least six times higher catalytic turnover than the bulk zeolites. A systematic catalytic investigation after the selective deactivation of internal or external Brönsted acid sites successfully showed that the higher catalytic performance of nanomorphic zeolite is due to the high portion of the external acid sites that are much more resistant to catalytic deactivation than the internal acid sites. Due to the presence of such catalytically valuable acid sites, nanomorphic zeolites are expected to be useful in a wide range of liquid-phase reactions including FC alkylation, which involve bulky species.

Acknowledgments

This work was supported by the Institute for Basic Science in Korea (IBS) [CA1301].

Appendix A. Supplementary data

Supplementary data associated with this article can be found, in the online version, at http://dx.doi.org/10.1016/j.apcata.2013.11.019.

References

[1] C. Friedel, J.M. Crafts, C.R. Hebd. Seances Acad. Sci. 84 (1877) 1450.
[2] G.A. Olah, Friedel–Crafts and Related Reactions, Wiley-Interscience, New York, NY, 1963.
[3] G.A. Olah, Friedel–Crafts Chemistry, Wiley, New York, NY, 1973.
[4] B. Viswanathan, B. Jacob, Catal. Rev. 47 (2005) 1–82.
[5] M.S. Khan, M.R.A. Al-Mandhary, M.K. Al-Suti, B. Ahrens, M.F. Mahon, L. Male, P.R. Raithby, C.E. Boothby, A. Kohler, Dalton Trans. 1 (2003) 74–84.
[6] I. Iovel, K. Mertins, J. Kischel, A. Zapf, M. Beller, Angew. Chem. Int. Ed. 44 (2005) 3913–3917.
[7] V.R. Choudhary, S.K. Jana, A.S. Mamman, Microporous Mesoporous Mater. 56 (2002) 65–71.
[8] V.R. Choudhary, S.K. Jana, J. Mol. Catal. A: Chem. 180 (2002) 267–276.
[9] K. Bachari, O. Cherifi, Catal. Commun. 7 (2006) 926–930.
[10] M.C. Clark, C.M. Smith, D.L. Stern, J.S. Beck, in: G. Ertl, H. Knözinger, F. Schüth, J. Weitkamp (Eds.), Handbook of Heterogeneous Catalysis, 7, Wiley-VCH, Weinheim, 2008, pp. 3153–3168.
[11] T.F. Degnan Jr., C.M. Smith, C.R. Venkat, Appl. Catal. A: Gen. 221 (2001) 283–294.
[12] M. Han, S. Lin, E. Roduner, Appl. Catal. A: Gen. 243 (2003) 175–184.
[13] P. Prokešová, N. Žilková, S. Mintova, T. Bein, J. Čejka, Appl. Catal. A: Gen. 281 (2005) 85–91.
[14] K.S.N. Reddy, B.S. Rao, V.P. Shiralkar, Appl. Catal. A: Gen. 95 (1993) 53–63.
[15] A.R. Pradhan, B.S. Rao, V.P. Shiralkar, in: G. Ohlmann, H. Pfeifer, R. Fricke (Eds.), Catalysis and Adsorption by Zeolites, 65, Elsevier, Amsterdam, 1991, p. 347.
[16] G. Bellussi, G. Pazzuconi, C. Perego, G. Girotti, G. Terzoni, J. Catal. 157 (1995) 227–234.
[17] Z. Liu, P. Moreau, F. Fajula, Appl. Catal. A: Gen. 159 (1997) 305–316.
[18] R. Roque-Malherbe, R. Wendelbo, A. Mifsud, A. Corma, J. Phys. Chem. B 99 (1995) 14064–14071.
[19] N. Narender, K.V.V.K. Mohan, S.J. Kulkarni, I.A.K. Reddy, Catal. Commun. 7 (2006) 583–588.
[20] Y. Sun, R. Prins, Appl. Catal. A: Gen. 336 (2008) 11–16.
[21] X. Li, R. Prins, J.A. van Bokhoven, J. Catal. 262 (2009) 257–265.
[22] H. Jin, M.B. Ansari, E.-Y. Jeong, S.-E. Park, J. Catal. 291 (2012) 55–62.
[23] S. Jun, R. Ryoo, J. Catal. 195 (2000) 237–243.
[24] N. Candu, M. Florea, S.M. Coman, V.I. Parvulescu, Appl. Catal. A: Gen. 393 (2011) 206–214.
[25] M. Guisnet, L. Costa, F.R. Ribeiro, J. Mol. Catal. A: Chem. 305 (2009) 69–83.
[26] M. Guisnet, P. Maagnoux, Appl. Catal. A: Gen. 54 (1989) 1–27.
[27] W. Kim, J.-C. Kim, J. Kim, Y. Seo, R. Ryoo, ACS Catal. 3 (2013) 192–195.
[28] J. Kim, W. Kim, Y. Seo, J.-C. Kim, R. Ryoo, J. Catal. 301 (2013) 187–197.
[29] F. Bauer, H.G. Karge, in: H.G. Karge, J. Weitkamp (Eds.), Molecular Sieves—Science and Technology, Characterization II, 5, Springer, Berlin, 2006, pp. 249–364.
[30] F. Bauer, W.H. Chen, E. Biiz, A. Freyer, V. Sauerland, S.B. Liu, J. Catal. 251 (2007) 258–270.
[31] K. Egeblad, C.H. Christensen, M. Kustova, C.H. Christensen, Chem. Mater. 20 (2008) 946–960.
[32] S. Ernst, P.A. Jacobs, J.A. Martens, J. Weitkamp, Zeolites 7 (1987) 458–462.
[33] W.F. Lai, W.J. Roth, R.E. Kay, C.N. Elia, (ExxonMobil) US 8003074, 2011.
[34] P.I. Ravikovitch, S.C.O. Domhnaill, A.V. Neimark, F. Schueth, K.K. Unger, Langmuir 11 (1995) 4765–4772.
[35] Y. Seo, K. Cho, Y. Jung, R. Ryoo, ACS Catal. 3 (2013) 713–720.
[36] P. Andy, J. Garcia-Martinez, G. Lee, H. Gonzalez, C.W. Jones, M.E. Davis, J. Catal. 192 (2000) 215–223.
[37] K. Na, C. Jo, J. Kim, K. Cho, J. Jung, Y. Seo, R.J. Messinger, B.F. Chmelka, R. Ryoo, Science 333 (2011) 328–332.
[38] E.F. Rakiewicz, A.W. Peters, R.F. Wormsbecher, K.J. Sutovich, K.T. Mueller, J. Phys. Chem. B 102 (1998) 2890–2896.
[39] Q. Zhao, W.-H. Chen, S.-J. Huang, Y.-C. Wu, H.-K. Lee, S.-B. Liu, J. Phys. Chem. B 106 (2002) 4462–4469.
[40] S. Van der beken, E. Dejaegere, K.A. Tehrani, J.S. Paul, P.A. Jacobs, G.V. Baron, J.F.M. Denayer, J. Catal. 235 (2005) 128–138.
[41] K. Mantri, K. Komura, Y. Kubota, Y. Sugi, J. Mol. Catal. A: Chem. 236 (2005) 168–175.
[42] V.R. Choudhary, S.K. Jana, N.S. Patil, S.K. Bhargava, Microporous Mesoporous Mater. 57 (2003) 21–35.